energy&fuels

pubs.acs.org/EF Article

Performance Evaluation of Inexpensive Cu/Fe-Based Oxygen Carriers in Chemical Looping Gasification of Coal

Yanan Wang, Hengfeng Bu, Haibo Zhao,* and Kunlei Liu

Cite This: *Energy Fuels* 2021, 35, 15513−15524 Read Online

ABSTRACT: Solid fuel chemical looping gasification (CLG) is an innovative syngas production technology that avoids expensive air separation requirements. However, solid fuel CLG requires the development of easily available, inexpensive oxygen carrier (OC) particles with tunable reactivity and good cycling performance. In this paper, the low-cost Cu/Fe-based OCs, derived from waste ore particles and/or bauxite residues, are comprehensively evaluated for potential coal-fed CLG application in a batch fluidized bed reactor. Among these OCs, the red mud and Cu20Fe80@C (16 wt % copper ore bonded with 64 wt % hematite by 20 wt % cement) OCs exhibit better CLG performances in terms of gasification time and syngas quality. Red mud exhibits promise for the Fischer−Tropsch synthesis, while Cu20Fe80@C is in favor of the H_2-rich chemical synthesis. Furthermore, coal and char gasification rates are closely related to both the lattice oxygen donation capacity and the alkali metal content in the OC, while the reduced OCs catalyze the conversion of gasification gas to the H_2-rich products. In addition, the reduced OCs behave differently during the water−gas shift (WGS) and steam−iron reactions (which factually provide an approach to tune the syngas quality) in a fixed bed reactor. Reduced Cu20Fe80@C exhibits high catalytic activity toward the WGS reaction, followed by reduced Fe100@C (80 wt % hematite bonded by 20 wt % cement) and reduced red mud. With regard to the H_2-rich production, the Cu20Fe80@C OC exhibits a clear advantage over red mud once both OCs experience deep reductions. Cyclic redox tests demonstrate that the red mud and Cu20Fe80@C OCs can achieve stable syngas production and exhibit good anti-sintering behavior.

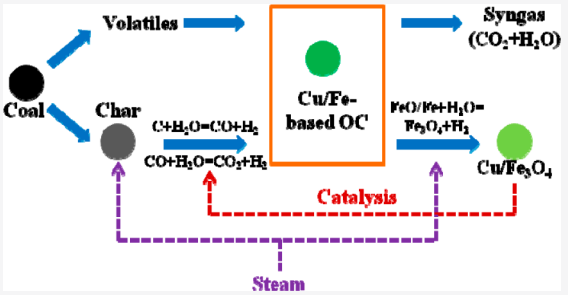

1. INTRODUCTION

Coal gasification technology has aroused increasing interest because it offers efficient and clean conversion of coal into syngas for power generation and chemical synthesis.[1,2] Nevertheless, conventional gasification technology faces many challenges, such as intensive capital requirements and high operating costs, both of which are caused by the need for a cryogenic air separation unit.[1−3] In view of this, chemical looping gasification (CLG) has emerged as a promising approach to syngas production via partial oxidation of solid fuel using an oxygen carrier (OC) that circulates between the air reactor and fuel reactor to transfer active oxygen and heat among them. This strategy shares the same basic principle as chemical looping combustion (CLC); however, the desired product is syngas rather than heat (and CO_2).[4]

As is the case with CLC, OC selection is a critical issue in CLG. Despite the different purposes of these two processes, they share the goals of tar yield reduction and carbon conversion improvement. Generally, the coal- and biomass-derived CLG processes tend to have higher tar yields than CLC because of its higher fuel/OC ratio.[5] Therefore, a desired OC for CLG should be capable of converting tar into syngas via reforming or catalytic cracking. Both synthetic and natural iron-based OCs have been investigated widely in the CLG mode because of their low costs, no toxicity, and low reactivities.[6,7] Virginie et al.[8] synthesized a Fe-based OC (Fe/olivine) and found that it could obviously reduce the biomass tar yield as a result of its burning function to volatile compounds and catalytic effects on tar/hydrocarbon reforming. Despite the small amount of carbon desposition formed on the OC surface, its structure remains stable during cycling. Samprón et al.[6] performed a biomass gasification investigation using a synthetic Fe-based OC in a continuous unit, and the results indicated that high-quality syngas as well as low tar content (below 2 g/Nm^3) could be achieved at autothermal conditions. Interestingly, when the synthetic Fe-based OCs were replaced with natural ilmenite or hematite, a notable tar removal efficiency could still be obtained with the aid of lattice oxygen and/or the catalytic abilities of natural materials.[7,9−12] For example, Condori et al.[9] used ilmenite as the OC for

Received: June 5, 2021
Revised: August 27, 2021
Published: September 9, 2021

https://doi.org/10.1021/acs.energyfuels.1c01800
Energy Fuels 2021, 35, 15513−15524

Table 1. Brief Summary of Main OCs Used in the Solid Fuel CLG Processes[a]

OC/preparation method	fuel	temperature (T)	facility	performance index	reference
Fe-based/WI	biomass	T = 820−940 °C	i-FBR	H_2/CO ratio of about 2 reached	6
hematite	coal	T = 865−915 °C	i-FBR	gasification process promoted with increasing temperature	7
Fe-based/LI	biomass	T = 750−850 °C	bs-FBR	65% tar reduction at 850 °C with OC	8
ilmenite	biomass	T = 820−940 °C	i-FBR	possible high-purity syngas production at autothermal conditions	9
ilmenite	coal	T = 900 °C	FiBR	no tar formed with preoxidized ilmenite	10
ilmenite	biomass	T = ∼825 °C	DFBG	about 50% tar reduction with 12 wt % ilmenite	12
Ba−Fe and Ca−Fe/SG	coal	T = ambient to 800−950 °C (200 °C/min) and ambient to 800 °C (4 °C/min)	TG and bs-FiBR	excellent gasification performance of both OCs	15
Ni−Fe/SG	biomass	T = ambient to 950 °C (10 °C/min) and 700−900 °C	TG and FiBR	flexible H_2/CO ratio achieved	17
Fe−M (M = Ba, Ca, Cu, Ni, and Co)/CP	coal	T = ambient to 900 °C (50 °C/min) and ambient to 800 °C (30 °C/min)	TG and ls-FiBR	improved syngas products with composite OCs	19
Cu−Fe/ME	biomass	T = 700−950 °C	b-FBR	superior carbon conversion efficiency of composite OC	20
Cu−Fe/SG	biomass	T = 500−900 °C	b-FBR	synergetic effect generated on the tar decomposition	21
Mn-, Fe-, Co-, and Ni-based/MS	coal	T = ambient to 900 °C and ambient to 800 °C (30 °C/min)	TG and bs-FiBR	improved coal gasification process with OCs	22
Cu−Fe/SG	biomass	T = ambient to 900 °C (20 °C/min) and 500−900 °C	TG and b-FBR	improved anti-sintering ability of Cu oxide by Fe_2O_3 addition	31

[a]WI, wetness impregnation; LI, liquid impregnation; SG, sol−gel; HT, hydrothermal; CP, co-precipitation; ME, mixing extrusion; MS, modified Stöber; i-FBR, interconnected fluidized bed reactor; bs-FBR, bench-scale fluidized bed reactor; FiBR, fixed bed reactor; DFBG, dual fluidized bed gasifier; bs-FiBR, bench-scale fixed bed reactor; ls-FiBR, lab-scale fixed bed reactor; b-FBR, batch fluidized bed reactor; and TG, thermogravimetry.

syngas production in a continuous unit and found that this technology exhibited an obvious advantage of tar removal (below 2 g/Nm^3) with respect to other syngas production processes. Also, natural bauxite exhibited promising tar reforming properties because of its high catalytic conversion of ethylene and relatively low coke formation.[13] Because composite OCs can integrate the advantages of various metal oxides, a series of additives was introduced into the pure iron oxides. Wang et al.[14] found that synthesized $CaFe_2O_4$ exhibited high reactivity for partial oxidation of toluene to syngas. Excellent reactivity of $CaFe_2O_4$ with coal and minimal reactivity with syngas were confirmed by Siriwardane et al.[15] Chen et al.[16] synthesized MFe_2O_4 (M = Cu, Ba, Ni, and Co) ferrites as OCs and observed that all of the ferrites exhibited good catalytic activities for toluene cracking because of synergetic effects between metal cations. He et al.[17] evaluated the $NiFe_2O_4$ OC as a catalyst for tar cracking and obtained syngas with a tar content of 2.83 g/m^3; the $NiFe_2O_4$ OC also demonstrated better reactivity and anti-deactivation properties than NiO or Fe_2O_3 alone.[18] Moreover, Kun et al.[19] found that Fe−Ni oxides also exhibited good reactivity with coal and high selectivity for syngas. Nevertheless, the disadvantages of Ni- and Co-based OCs, such as their high cost and toxicity, have helped Cu−Fe bimetallic OCs attract more attention. Shen et al.[20] reported that the combined Cu−Fe OCs demonstrated catalytic effects on biomass gasification and tar cracking processes that resulted in the improved carbon conversion. Tian et al.[21] investigated the use of Cu−Fe composite oxides as OCs during the biomass-derived CLG processes and clearly identified the respective roles of Cu and Fe in promoting tar conversion: the Cu component helped to break down small molecular compounds, while Fe could decrease the yield of large molecular compounds.

Besides tar breakdown, the char gasification as the rate-limiting step within the whole CLG processes should be considerably accelerated. Factually, either the fast reaction between the OC and pyrolysis/gasification products or the slow direct solid−solid reaction between coal and the OC is conducive to the improvement of the overall char gasification process more or less;[16,22] however, their contribution is far below expections. O_2 uncoupling materials, such as Cu- and Mn-based OCs, have attracted attention because the presence of lean O_2 released by these materials in the fuel reactor can accelerate the char conversion several times.[23,24] Because pure manganese oxide does not perform satisfactorily in CLC of coal,[25] the mixed Mn−Fe oxides have been developed recently as OCs. However, there has to be an obvious temperature difference betweeen the fuel reactor and air reactor.[26] Cu-based materials have been investigated widely as a result of their high reactivity,[27,28] but the low melting point and "too" fast oxygen transfer ability of Cu oxides[29,30] limit their independent implementation in CLG. Considering the medium reactivity and high melting point of Fe_2O_3, the various combinations of Fe_2O_3 and CuO, i.e., bimetallic Cu−Fe oxides, have been introduced as promising OCs into the CLG mode. Shen et al.[20] found that the combined Cu−Fe oxide OCs could enhance the coal gasification rate significantly more than pure Fe_2O_3 during the CLG process. The Fe_2O_3/CuO blending weight ratio used in the combined OC was optimized to 50:10 after taking the syngas yield, carbon conversion efficiency, and gasification rate into consideration. In contrast, Niu et al.[31] found that, in the biomass CLC process, the best molar ratio of CuO/Fe_2O_3 was 50:50 based on a comprehensive evaluation of the product gas components, carbon conversion, gas yield, and tar yield.

https://doi.org/10.1021/acs.energyfuels.1c01800
Energy Fuels 2021, 35, 15513−15524

Table 2. Raw Material Compositions of Prepared OCs

							Fe100@C		Cu20Fe80@C		Cu10.9Red89.1@C	
copper ore	wt %	hematite	wt %	red mud	wt %	cement	wt %	component	wt %	component	wt %	component	wt %
CuO	21.0	Fe_2O_3	87.2	Fe_2O_3	42.6	Al_2O_3	44.0	hematite	80.0	copper ore	16.0	copper ore	8.7
$CuFe_2O_4$	70.1	SiO_2	7.8	Na_2O	6.6	CaO	38.9	cement	20.0	hematite	64.0	red mud	71.3
SiO_2	5.5	Al_2O_3	3.9	Al_2O_3	22.5	SiO_2	10.3			cement	20.0	cement	20.0
others	3.4	others	1.1	others	28.3	others	6.8						

Table 3. Proximate and Ultimate Analyses of Lignite/Char

	proximate analysis (wt %, ad)				ultimate analysis (wt %, ad)			
solid fuel	moisture	volatiles	ash	fixed carbon	C	H	N	S
CF	2.66	42.62	16.29	38.43	54.58	3.91	0.93	1.79
CF char	1.25	9.41	29.23	60.11	65.25	1.15	0.75	1.02

It is notewarthy that catalytic alkali and alkaline earth metal (AAEM) components have been introduced into the chemical looping system to improve the char gasification rate, mainly through two ways: one is to modify the solid fuel with AAEM, and the other is to modify the OC with AAEM. As for the first method, Yang et al.[32] found that the impregnation of K or Ca into raw coal can significantly accelerate the char gasification process, reducing the gasification time from 50 min of raw char at 1173 K to 15 min of K impregnation and 30 min of Ca impregnation at 1123 K. Moreover, Wang et al.[33] concluded that K impregnation improved the char gasification because of its inhibition effect on the graphitization of petcoke, and the water−gas shift (WGS) reaction can also be promoted by the generated catalytic intermediates. As for the second method, Guo et al.[34] reported that the CaO addition to iron-based OC improved both the coal gasification rate and the carbon conversion efficiency, which was attributed to the catalytic effects of CaO. Excitingly, cheap red mud waste from the alumina industry has been confimed to play a catalytic role in char gasification as a result of it containing Na.[35] This is consistent with observations by Arjmand et al.[36] To couple the contribution of alkali metal into cement-bonded Cu−Fe OC, cement-bonded copper ore and red mud OC has been tested, which presented both high reactivity and good contribution in CLC mode.[28,37]

To summarize, the Cu−Fe composite OCs are excellent candidates with regard to the tar reduction and char gasification improvement, which is the intention as to why Cu−Fe composite OCs are chosen as OC candidates during the coal CLG process in this study. Table 1 summarizes the detailed information on the above-mentioned OCs using coal or biomass as fuel. Through detailed analysis and comparison, we proposed the following points to design the OC, to improve its comprehensive performance in CLG/CLC of coal. First, natural ores or industrial wastes are advatageous raw materials with regard to cost and environmental friendliness. Second, cement is used as a binder to combine fine raw particles into single targeted particles and also improves the sintering resistance ability of OC. Third, catalytic AAEM components can be introduced into OC particles to help improve the char gasification rate. In view of the above points, the cement-bonded fine copper ore and hematite particles as OC and the cement-bonded fine copper ore and red mud particles as OC have been developed by our group, and these OCs did exhibit outstanding reactivity in the CLC mode,[28,37−39] which deserves further test in the CLG mode.

In this study, the low-cost Cu/Fe-based OCs, prepared from natural ores and/or red mud, are first investigated in the CLG mode of lignite. The gas distribution characteristics (concentration curves for each gas and overall gas compositions) and syngas quality (syngas yield, H_2/CO ratio, and lower heating value) of the OCs are analyzed comparatively, and then the copper ore/hematite blending weight ratio in the OC is further optimized. Also, the role of lattice oxygen and alkali metal in promoting coal gasification and the role of the reduced OCs in catalyzing the H_2-rich syngas production are explored in detail by well-designed experiments, respectively. Moreover, the regulating effects of the WGS and steam−iron reactions are both investigated in a fixed bed reactor. In addition, cyclic tests are further performed for optimized OCs of red mud and Cu20Fe80@C.

2. MATERIALS AND METHODS

2.1. Material Preparation. *2.1.1. OC Preparation.* Fine particles of natural copper ore and hematite (or red mud) are used as raw materials (see the detailed compositions in Table 2) for the preparation of composite OCs. In our notation system, Cu20Fe80@C and Cu10.9Red89.1@C represent that the mixing weight ratios of copper ore (marked as Cu) to hematite (marked as Fe) and copper ore to red mud (marked as Red) in the OCs are 20:80 and 10.9:89.1, respectively, and the binder of cement (marked as C) added to the prepared OC always accounts for 20 wt %. These weight ratios are determined on the basis of our previous investigation,[37,40] and the detailed preparation process can be seen in ref 37. Moreover, the red mud and Fe100@C (representing 80 wt % hematite bonded with 20 wt % cement) OCs are also prepared. All OCs used for tests are in the size range of 0.15−0.35 mm.

2.1.2. Fuel Preparation. The lignite used in the tests comes from Inner Mongolia, China. Before use, it is dried in a drying oven at 105 °C for 24 h to remove internal and external water. Then, particles in the size range of 0.2−0.3 mm are selected for use. Lignite char particles with the same size are prepared for further testing. Char particles are obtained after cracking treatment at 950 °C in a continuous N_2 flow. The proximate and ultimate analyses of the lignite and its char are listed in Table 3.

2.2. Experimental Section. A batch fluidized bed reactor system[37] is used for the lignite or lignite char tests. The reactor is heated on the basis of the feedback from the thermocouple in the furnace chamber, while another thermocouple inside the tube monitors the real reaction zone temperature. During the reduction period, the feeding mass of lignite (or its char) is 0.90 g (or 0.78 g), respectively. All tests are performed at 950 °C, and the flow rate of the fluidization gas is controlled at 2 L/min (0.8 g/min H_2O + 1 L/min N_2). To be noted, for the copper-ore-containing OCs, the lignite or its char particles are quickly introduced into the reactor when the O_2 concentration in gas phase decreases to 1.5% (obtained from the pre-

https://doi.org/10.1021/acs.energyfuels.1c01800
Energy Fuels 2021, 35, 15513−15524

Table 4. Summary of Operational Conditions in the Fluidized/Fixed Bed Reactor

part of tests	bed material	fuel type	fuel feeding mass (g) or rate (mL/min)	temperature (°C)	O/C ratio	inlet gas
first	Fe100@C	lignite	0.90	950	0.5	50% H_2O + 50% N_2
	red mud	lignite	0.90	950	0.5	50% H_2O + 50% N_2
	Cu20Fe80@C	lignite	0.90	950	0.5	50% H_2O + 50% N_2
	Cu10.9Red89.1@C	lignite	0.90	950	0.5	50% H_2O + 50% N_2
second	Fe100@C	lignite	0.90	950	0.2	50% H_2O + 50% N_2
	red mud	lignite	0.90	950	0.2	50% H_2O + 50% N_2
	Cu20Fe80@C	lignite	0.90	950	0.2	50% H_2O + 50% N_2
	Fe100@C	char	0.78	950	0.5	50% H_2O + 50% N_2
	red mud	char	0.78	950	0.5	50% H_2O + 50% N_2
	Cu20Fe80@C	char	0.78	950	0.5	50% H_2O + 50% N_2
	re-Fe100@C	char	0.78	950		50% H_2O + 50% N_2
	re-red mud	char	0.78	950		50% H_2O + 50% N_2
	re-Cu20Fe80@C	char	0.78	950		50% H_2O + 50% N_2
third	re-Fe100@C	CO	40	550−950		10% CO + 40% H_2O + 50% N_2
	re-red mud	CO	40	550−950		10% CO + 40% H_2O + 50% N_2
	re-Cu20Fe80@C	CO	40	550−950		10% CO + 40% H_2O + 50% N_2
	SiO_2	CO	40	650−950		10% CO + 40% H_2O + 50% N_2
	dre-Fe100@C	CO	60	950		40% H_2O + 60% N_2
	dre-red mud	CO	60	950		40% H_2O + 60% N_2
	dre-Cu20Fe80@C	CO	60	950		40% H_2O + 60% N_2
	dre-Cu10.9Red89.1@C	CO	60	950		40% H_2O + 60% N_2
fourth (cyclic tests)	red mud	lignite	0.90	950	0.2	50% H_2O + 50% N_2
	Cu20Fe80@C	lignite	0.90	950	0.2	50% H_2O + 50% N_2

experiment). To recover the reduced OC for the next test, air with a flow rate of 1 L/min is used as oxidation gas. The flue gas from the reactor outlet is passed through a filter and cooler to remove fine particles and water, respectively, and then enters an online gas analyzer (Gasboard Analyzer 3100) for real-time detection of gas concentrations.

Four parts of experiments are conducted. The operational conditions for the fluidized/fixed bed tests are listed in Table 4, where each test is repeated 3 times. The purpose of the first part of experiments is to evaluate the coal gasification performance under various OCs. Here, to ensure the same amount of available lattice oxygen from different OCs (considering the reduction of CuO/Fe_2O_3 to Cu_2O/Fe_3O_4, respectively) and same bed height for different bed materials, inert sand is used as the balance material. Therefore, the bed materials used in the CLG tests are 30.53 g of Fe100@C with 48.86 g of sand, 50 g of red mud with 40.31 g of sand, 25.19 g of Cu20Fe80@C with 53.89 g of sand, and 46.28 g of Cu10.9Red89.1@C with 28.42 g of sand, respectively. Each test corresponds to an O/C ratio of 0.5 with 0.90 g of lignite being used as fuel. As a result of the advantage of copper-ore-contaning OCs (Cu20Fe80@C and Cu10.9Red89.1@C) over respective single material OC (Fe100@C or red mud) in the coal conversion rate, composite OCs with improved copper ore/hematite mixing weight ratios are further tested.

The second part of experiments is designed to investigate (1) the role of lattice oxygen and alkali metal in promoting the carbon conversion and (2) the effect of the reduced OCs (labeled re-OCs) on catalyzing the H_2-rich syngas production without lattice oxygen interference. As for the target 1, lignite (or its char) experiments are performed using an O/C ratio of 0.2 (or 0.5). When the oxygen/fuel ratio is 0.2, the bed materials used are 12.21 g of Fe100@C with 65.70 g of sand, 20 g of red mud with 62.28 g of sand, and 10.07 g of Cu20Fe80@C with 67.72 g of sand, respectively. To be noted, the re-OCs are obtained at the end of char reduction tests (an O/C ratio of 0.5), without an oxidation step, and the same mass of char is again added to identify the catalytic effect in the target 2 test. Two continuous char additions can be regarded as pulsed feeding.

The third part of experiments is to investigate the (1) catalytic effects of re-OCs on the WGS reaction and (2) H_2 production charateristics of deeply reduced OC (labeled dre-OC). All tests are conducted in a fixed bed reactor with a diameter of 30 mm and height of 750 mm. For the WGS reaction, all re-OCs are obtained at the end of the first char tests of pulsed feeding (the target 1 test). The masses of re-red mud, red-Fe100@C, and re-Cu20Fe80@C are determined as 16, 9.68, and 10.54 g, respectively, keeping the same theoretic mass of Fe_2O_3 (6.92 g) in initial OCs (oxidation state). To be noted, re-Cu20Fe80@C theoretically contains not only 6.69 g of Fe_3O_4 but also 0.62 g of Cu. The inert sand as the balance material added to the re-red mud, red-Fe100@C, and re-Cu20Fe80@C is 3.52, 5.53, and 4.56 g, respectively. The total flow rate of inlet gas is controlled to 400 mL/min. For the steam−iron reaction, Fe100@C, red mud, Cu20Fe80@C, and Cu10.9Red89.1@C with the same mass of 10 g are used as bed materials, respectively. CO (10 vol %) balanced by N_2 with a total flow rate of 600 mL/min is used as the reduced gas to produce deeply reduced OC (labeled dre-OC). After the reduction step, pure N_2 with a flow rate of 600 mL/min is used as a sweeping gas to remove remaining CO from the reactor and pipe. Then, 40 vol % steam balanced by N_2 with a total flow rate of 600 mL/min is used as an oxidation gas for H_2 production.

The fourth part of experiments aims to evaluate the cyclic stability of preferred OCs for syngas production. Moreover, environmental scanning electron microscopy (ESEM, Quanta 200) together with energy-dispersive X-ray spectroscopy (EDX) are used to character the fresh and used OCs.

2.3. Data Evaluation. The specific formulas employed to evaluate the CLG results are summarized in Table 5.

3. RESULTS AND DISCUSSION

The coal-derived CLG process is achieved by controlling the O/C ratio in the range of 0−1.0, which is between coal-derived CLC (an O/C ratio greater than or equal to 1.0) and steam−coal external gasification (an O/C ratio of 0). During the CLG process, insufficient active bed material can burn off partial intermediate syngas from the steam−coal gasification reaction. Because the combustion reactions are usually exothermic, they provide a feasible route toward achieving autothermal coal gasification and also play a role in regulating the syngas quality.

https://doi.org/10.1021/acs.energyfuels.1c01800
Energy Fuels 2021, 35, 15513−15524

Table 5. Summary of Evaluation Formulas

item	formula[a]
oxygen/fuel ratio	$O/C = \frac{R_{OC} m_{OC}}{\varphi_{OC} m_{fuel}}$ (1)
gas volume fraction	$V_i = \frac{\int_{t_0}^{t_{total}} F_{out,red} y_i \, dt}{\int_{t_0}^{t_{total}} F_{out,red}(y_{CO} + y_{CO_2} + y_{H_2} + y_{CH_4}) dt}$ (2)
outlet gas flow rate (s^{-1})	$F_{out,red} = \frac{F_{N_2}}{1 - y_{CO_2} - y_{CO} - y_{CH_4} - y_{H_2} - y_{O_2}}$ (3)
syngas yield (Nm^3/kg of fuel)	$G_{syn} = \frac{\int_{t_0}^{t_{total}} F_{out,red}(y_{CO} + y_{CH_4} + y_{H_2}) dt}{m_{fuel}}$ (4)
H_2/CO ratio	$\gamma = V_{H_2}/V_{CO}$ (5)
lower heating value of gas products (MJ/Nm^3)	$LHV = 12.64V_{CO} + 35.88V_{CH_4} + 10.79V_{H_2}$ (6)
carbon conversion	$X_c = \frac{\int_{t_0}^{t} F_{out,red}(y_{CO_2} + y_{CO} + y_{CH_4}) dt}{\int_{t_0}^{t_{total}} F_{out,red}(y_{CO_2} + y_{CO} + y_{CH_4}) dt}$ (7)
instantaneous carbon conversion rate (s^{-1})	$x_{inst} = \frac{1}{1 - X_c} \frac{dX_c}{dt}$ (8)
oxygen transfer rate of OC[37] (g/s)	$r_{OC} = \frac{16 F_{out,red}(2y_{CO_2} + 2y_{O_2} + y_{CO} - y_{H_2})}{22.4}$ (9)
experimental equilibrium constant[41]	$K = \frac{X_{CO}^2}{(1 - X_{CO})(\lambda - X_{CO})}$ (10)
H_2 production rate from the steam−iron reaction (s^{-1})	$F_{H_2} = F_{out,red} y_{H_2}$ (11)
total H_2 yield from the steam−iron reaction (mol)	$G_{H_2} = \frac{\int_{t_0}^{t_{total}} F_{out,red} y_{H_2} \, dt}{22.4}$ (12)

[a] R_{OC}, oxygen loading capacity of OC reduced from Fe_2O_3/CuO to Fe_3O_4/Cu_2O;[38] φ_{OC}, oxygen demand as per unit mass fuel fully converted into CO_2 and H_2O; m_{OC}, OC mass; m_{fuel}, fuel mass; $F_{out,red}$, outlet gas flow rate; t_0, beginning time of the reduction period; t_{total}, ending time of the reduction period; y_i, instantaneous volume concentration of each gas i in the outlet; F_{N_2}, inlet N_2 flow rate; ω_c, carbon content in the raw coal; X_{CO}, CO conversion at different conditions; and λ, molar ratio of H_2O/CO in the feeding gas.

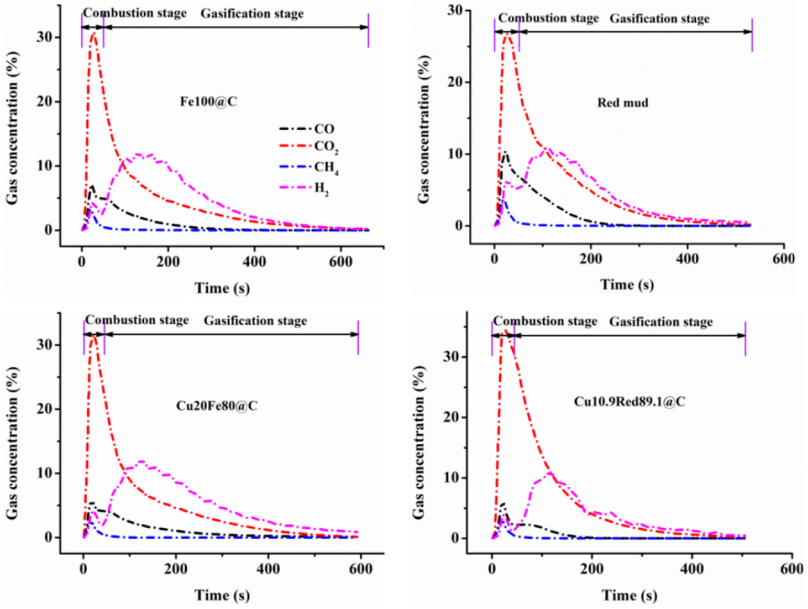

Figure 1. Concentration profiles of different OCs during CLG tests (temperature, 950 °C; O/C ratio, 0.5; and steam concentration, 50 vol %).

3.1. Function of OC. Figure 1 shows the concentration profiles of four OCs at an O/C ratio of 0.5. The CLG process of each OC consists of two stages, combustion and gasification, which can be distinguished clearly from the distribution of the

https://doi.org/10.1021/acs.energyfuels.1c01800
Energy Fuels 2021, 35, 15513−15524

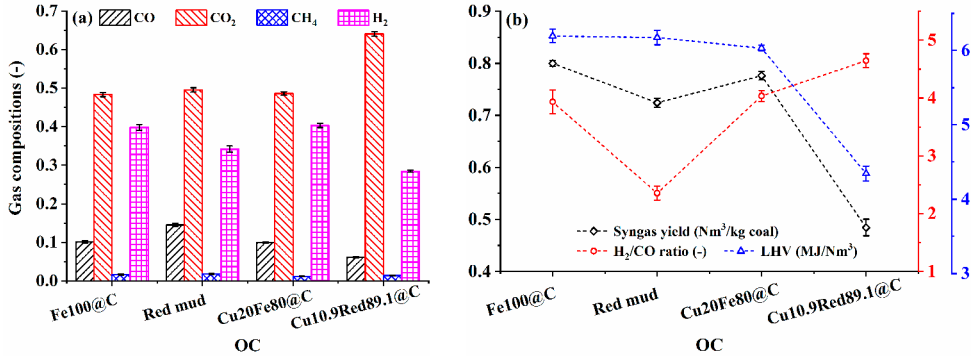

Figure 2. (a) Gas compositions and (b) syngas quality from various OCs during the CLG tests (temperature, 950 °C; O/C ratio, 0.5; and steam concentration, 50 vol %).

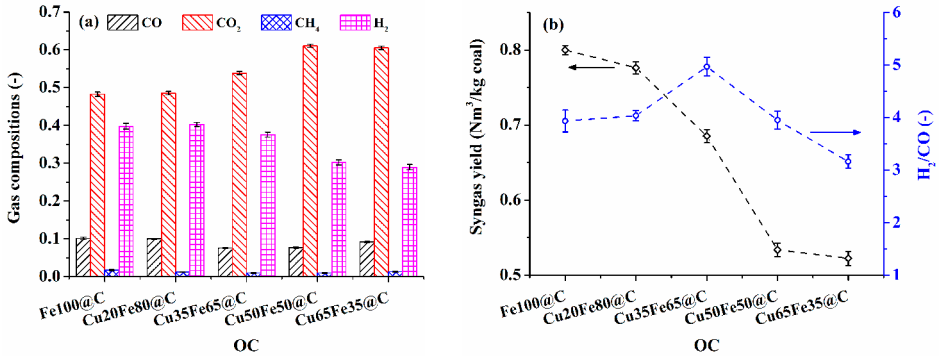

Figure 3. (a) Gas compositions and (b) syngas quality when OCs with various copper ore contents are used in CLG tests (temperature, 950 °C; O/C ratio, 0.5; and steam concentration, 50 vol %).

two H_2 peaks. At the first stage, most of volatiles/gasification gases, such as CO, CH_4, and H_2, are converted to CO_2 and H_2O via OC reduction. At the second stage, the CO concentration presents much lower than the CO_2 and H_2 concentrations after the first few seconds, while the H_2 concentration first increases and then exceeds the CO_2 curve. Next, the two gas concentrations maintain a similar decreasing trend. It is noted that the first stage lasts for a shorter time (about 50 s), while the duration of the second-stage reaction is several times longer. This indicates that the char gasification is indeed the rate-limiting step in the CLG process.

In comparison to Fe100@C, Cu20Fe80@C exhibits higher reactivity with volatiles/gasification gases during the combustion stage, which can be reflected directly from its higher CO_2 peak and lower CO, H_2, and CH_4 peaks. With respect to the gasification period, two main reactions occur: char−steam gasification and OC reduction. Because steam is used as the gasifying agent, the WGS reaction is always present, which can be confirmed by the higher H_2 concentration relative to CO at the end of the gasification period, when lattice oxygen in the OC has been basically exhausted according to later X-ray diffraction (XRD) patterns. By comparison of the red mud and Cu10.9Red89.1@C OCs, it is found that Cu10.9Red89.1@C consumes more combustible gas in comparison to red mud during the combustion period: it produces a lower flammable gas concentration and a higher CO_2 concentration. However, the H_2 peaks of Cu10.9Red89.1@C and red mud are similar during the gasification period: 10.93 and 10.90%, respectively. It can be inferred that the addition of copper ore significantly improves the combustion performance during the combustion period but generates little effect on the gas concentration distribution of the gasification period. To be noted, the copper-ore-containing OCs exhibit a shorter reaction time in comparison to their respective single-material OCs, i.e., 664 s for Fe100@C versus 592 s for Cu20Fe80@C and 530 s for red mud versus 505 s for Cu10.9Red89.1@C, which may be attributed to the contribution of the direct lean O_2−char reaction. The shorter reaction durations of red mud and Cu10.9Red89.1@C than those of Fe100@C and Cu20Fe80@C, respectively, can be explained by the presence of alkali metal, which is believed to catalyze the char conversion.

The gas compositions of the above-mentioned four OCs are shown in Figure 2a. The resultant gas composition with Fe100@C is similar to that with Cu20Fe80@C. However, there is a large difference between red mud and Cu10.9Red89.1@C OCs in the gas compositions, especially with regard to CO_2 (0.49 of red mud versus 0.64 of Cu10.9Red89.1@C). This may be attributed to the better reactivity of Cu10.9Red89.1@C relative to pure red mud with volatiles/gasification gases, as presented in ref 37. Also, the total oxygen loss amounts from Cu10.9Red89.1@C and red mud are calculated to be 0.97 and 0.79 g, respectively, based on the calculation method in refs 37 and 42. They exceed the theoretical value of 0.71 g (assuming that Fe_2O_3 is reduced to Fe_3O_4). This is because, as the Fe-based phases are reduced to a deeper FeO or Fe state, it is difficult to completely recover Fe_3O_4 in a steam environment.[43]

As seen in Figure 2b, the syngas yield with red mud is significantly higher than that with Cu10.9Red89.1@C. Thus, the cement-bonded red mud and copper ore fine particles as OC, i.e., Cu10.9Red89.1@C, is not a good OC candidate for

https://doi.org/10.1021/acs.energyfuels.1c01800
Energy Fuels 2021, 35, 15513−15524

CLG because it converts more syngas to CO_2 and H_2O than red mud. In contrast, the Cu20Fe80@C OC produces only a slightly lower syngas yield and lower heating value (LHV) than Fe100@C, but the shorter reaction time of Cu20Fe80@C exhibits its superiority. With respect to the H_2/CO ratio, the red mud OC attains a value of 2.36, which exceeds the requirement for the Fischer−Tropsch synthesis slightly. The ratios for Fe100@C and Cu20Fe80@C are 3.93 and 4.03, respectively, and are good for producing H_2-rich syngas.

To optimize the copper ore proportion in the cement-bonded hematite and copper ore OC, Cu35Fe65@C, Cu50Fe50@C, and Cu65Fe35@C are further tested. The resulting gas distributions are presented in Figure 3a. It is found that the CO_2 content rises obviously when the weight ratio of copper ore/hematite increases from 20:80 to 50:50, which results in a significant decrease of the syngas yield, as shown in Figure 3b. Hence, it can be concluded that a further increase in the copper ore/hematite weight ratio from 20:80 will not be appropriate for syngas production. Except for the higher H_2/CO ratio of 4.97 obtained using Cu35Fe65@C, the other OCs maintain ratios of 3.0−4.0. On the basis of the above results, Cu20Fe80@C is selected from the copper-ore-hematite mixed OCs for further study.

3.2. Promoting Role for Carbon Conversion and H_2-Rich Syngas Production. *3.2.1. Active Effects of Lattice Oxygen and Alkali Metal on the Carbon Conversion Rate.* The instantaneous carbon conversion rates (x_{inst}) of Fe100@C, red mud, and Cu20Fe80@C at various O/C ratios are shown in Figure 4. The results indicate that the x_{inst} value increases as

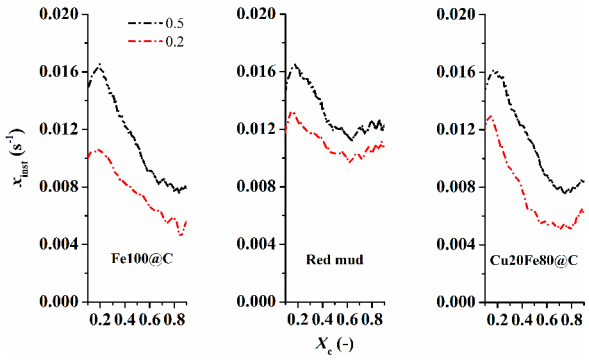

Figure 4. Instantaneous carbon conversion rate (x_{inst}) of different OCs at O/C ratios of 0.5 and 0.2 during CLG tests (temperature, 950 °C; steam concentration, 50 vol %).

the O/C ratio rises from 0.2 to 0.5 for each OC. The reasons can be summarized into categories. First, a larger bed inventory can cause more flammable gas to be consumed; these exothermic gas−solid reactions will accelerate the endothermic coal gasification process. Moreover, OC as a lattice oxygen donor can convert partial tar products into small molecule carbon-containing gases during the coal pyrolysis period, which explains why a higher x_{inst} is attained at a larger O/C ratio during the early carbon conversion period. Second, because H_2 is considered as the inhibitor for the char−steam reaction,[44,45] a lower H_2 yield at an O/C ratio of 0.5 can benefit the char gasification when compared to an O/C ratio of 0.2. In addition, the x_{inst} values attained with two O/C ratios of 0.2 and 0.5 are compared to that with an O/C ratio of 2.5 shown in ref 37. It can be concluded that the lower the O/C ratio, the smaller the x_{inst} value. This further validates the promoting effect of active lattice oxygen on coal conversion. To be noted, the red mud OC always exhibits higher x_{inst} values than Fe100@C and Cu20Fe80@C during the later carbon conversion period, which can be explained by the catalytic function of the alkali metal Na^+ from the red mud.

Here, the first char experiments of pulsed feeding (labeled G1) are performed; the x_{inst} values at various OCs are shown in Figure 5. As seen, when the carbon conversion is less than

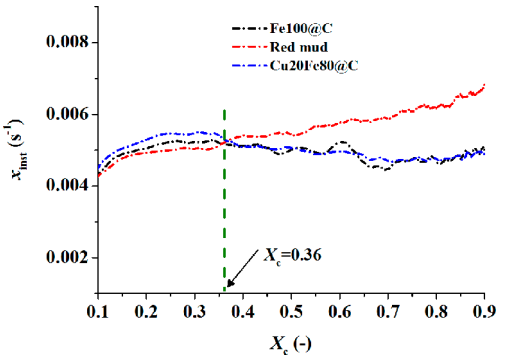

Figure 5. Instantaneous carbon conversion rate (x_{inst}) of different OCs during the first char tests (temperature, 950 °C; O/C ratio, 0.5; and steam concentration, 50 vol %).

0.36, the x_{inst} values of different OCs follow the order: Cu20Fe80@C > Fe100@C > red mud. Meanwhile, according to eq 9, the total oxygen loss amount from each OC is calculated within the interval of X_c = 0.10−0.36, that is, 0.41 g for Cu20Fe80@C, 0.37 g for Fe100@C, and 0.30 g for red mud. This demonstrates that the lattice oxygen indeed promotes the coal char conversion step. However, the red mud surpasses other two OCs in terms of x_{inst} once X_c exceeds 0.36, which is attributed to the alkali metal catalytic contribution.

3.2.2. Catalytic Effect of Reduced OCs on the H_2-Rich Syngas Production. After the first char tests of pulsed feeding, the total oxygen loss amount from each OC is calculated. They are 0.78 g for Cu20Fe80@C, 0.65 g for Fe100@C, and 0.63 g for red mud. These either exceed or approach the theoretical value of 0.71 g. This means that the reduced OCs (re-OCs) can be obtained at the end of the first char tests, as confirmed from the XRD patterns in Figure 6a. Then, the second char tests of pulsed feeding (labeled as G2) are performed. Figure 6b compares the x_{inst} values based on various re-OCs; it is found that the re-red mud always maintains a superior x_{inst} in comparison to the other two re-OCs throughout the coal char conversion process, which can be seen as a continuation of the advantageous x_{inst} at the later portion of the first series of tests.

As shown in Figure 6b, the two x_{inst} curves of re-Fe100@C and re-Cu20Fe80@C intersect at X_c = 0.71. The accumulated H_2 yields in two zones (X_c = 0.10−0.71 and 0.71−0.90) are calculated for these two re-OCs, as shown in Figure 7. The resulting H_2 yield of re-Fe100@C (0.664 L) is lower than that of re-Cu20Fe80@C (0.792 L) at X_c = 0.10−0.71, but the situation is reversed at X_c = 0.71−0.90 (0.369 L with re-Fe100@C versus 0.342 L with re-Cu20Fe80@C). Together with the x_{inst} curves, one can infer that a higher H_2 yield is associated with a lower x_{inst}. This is because the effect of H_2 inhibition hinders the char gasification at a higher rate.[44] It is observed that the re-red mud OC always maintains a higher x_{inst} than the other two re-OCs, which can be attributed to the

https://doi.org/10.1021/acs.energyfuels.1c01800
Energy Fuels 2021, 35, 15513−15524

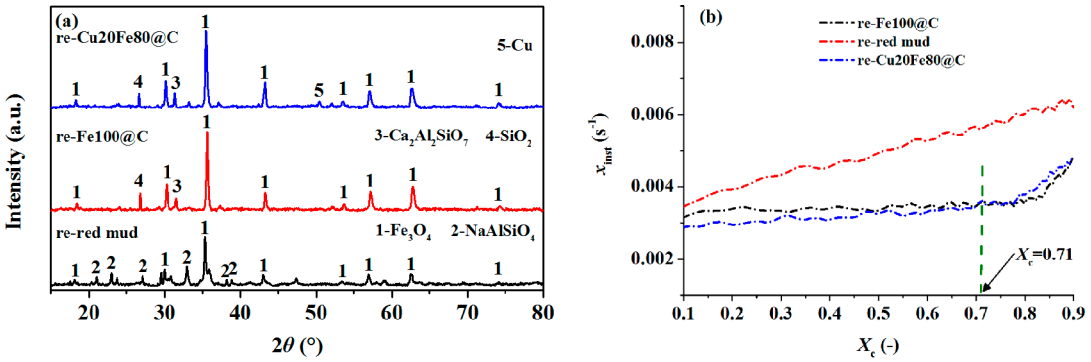

Figure 6. (a) XRD patterns of the reduced OCs and (b) instantaneous carbon conversion rate (x_{inst}) of various re-OCs (temperature, 950 °C; steam concentration, 50 vol %).

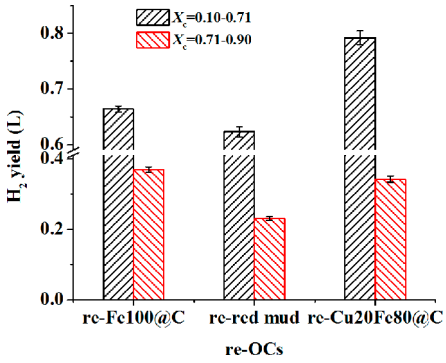

Figure 7. Accumulated H_2 yield at different carbon conversion zones based on different re-OCs (temperature, 950 °C; steam concentration, 50 vol %).

contributions from both alkali metal and the lower concentration of H_2 inhibitor.

The syngas quality is also evaluated for the char experiments with pulsed feeding. Figure 8a indicates that the G2 process obtains a lower CO_2 content, higher CO and H_2 contents, and longer reaction time (the number in parentheses) in comparison to the G1 process for each OC, which is mainly because the remaining lattice oxygen is negligible at the end of the G1 process. In the G2 process, it is found that re-red mud presents higher CO and lower H_2 contents when compared to either of the other two re-OCs. This may be attributed to the weaker catalytic effect of the re-red mud OC on the syngas reforming reaction. The detailed syngas yields and H_2/CO ratios for two processes are calculated and shown in Figure 8b.

The results indicate that the syngas yield with the G1 process is significantly lower than that with the G2 process for each OC, which is consistent with the results shown in Figure 8a. Moreover, it is noted that the H_2/CO ratios with various re-OCs follow the order: re-Fe100@C > re-Cu20Fe80@C > re-red mud in the G2 process, where the H_2/CO ratio is highly related to the WGS reaction. Thus, it can be inferred that re-Fe100@C and re-Cu20Fe80@C can exhibit a better catalytic function in the WGS reaction in comparison to re-red mud, which is further validated in section 3.3.1, while the lower H_2/CO ratio of re-Cu20Fe80@C than re-Fe100@C may be due to the less mass of active Fe_3O_4 contained in re-Cu20Fe80@C (in theory, 15.41 g of Fe_3O_4 in re-Cu20Fe80@C and 20.60 g of Fe_3O_4 in re-Fe100@C).

3.3. Regulating Roles of the WGS and Steam−Iron Reactions. *3.3.1. Catalytic Function of Reduced OCs during the WGS Reaction.* The second char tests of pulsed feeding reveal possible catalytic differences of various reduced OCs in the WGS reaction. Further detailed investigations of the catalytic effects of reduced OCs on the WGS reaction are conducted. Three reduced OCs and inert sand are used as bed materials, and the operating temperature ranges from 550 to 950 °C. Figure 9 shows that the experimental equilibrium constants of all three reduced OCs are far larger than that of inert sand (at least 30 times higher even at 950 °C with a minimum gap), indicating the higher catalytic activity of the reduced OCs. The equilibrium constant of each reduced OC rises dramatically as the temperature increases from 550 to 750 °C, and the order of equilibrium constants for all reduced OCs is re-Cu20Fe80@C > re-Fe100@C > re-red mud across this

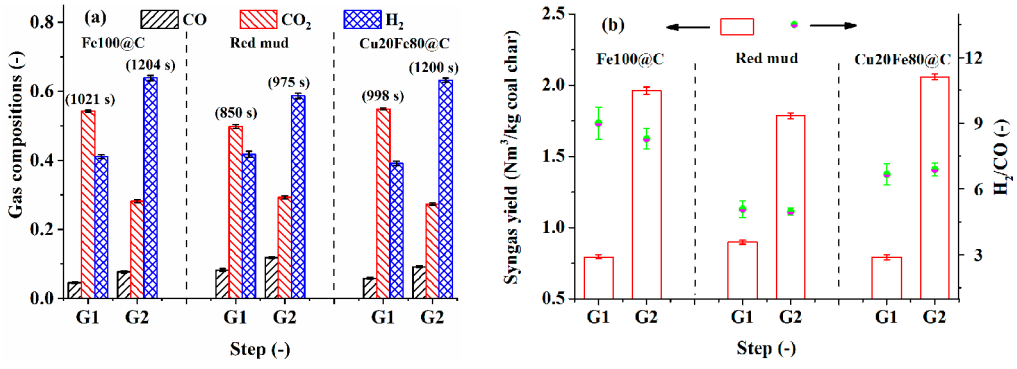

Figure 8. (a) Gas compositions and (b) syngas quality of various OCs during the two series of tests (temperature, 950 °C; steam concentration, 50 vol %; the number in parentheses is the average reaction time for three repeated tests).

https://doi.org/10.1021/acs.energyfuels.1c01800
Energy Fuels 2021, 35, 15513−15524

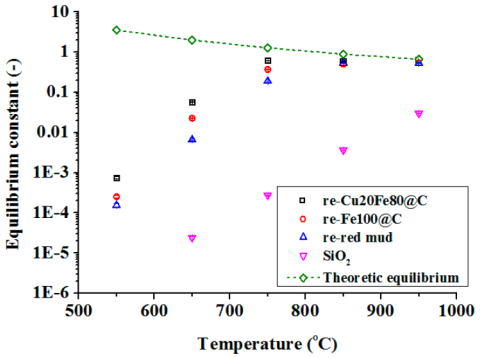

Figure 9. Equilibrium constant of different re-OCs at various temperatures.

temperature range. Thus, re-Cu20Fe80@C can exert a stronger catalytic effect than either of the other two reduced OCs, which helps to reach an equilibrium state at a lower temperature. When the reaction temperature further rises to 850 °C, the difference between the experimental and theoretic equilibrium constants shrinks, that is to say, a high temperature helps the WGS reaction to reach its theoretical equilibrium state.

3.3.2. H_2 Production via the Steam−Iron Reaction. In the CLG process, deep reduction occurs easily as a result of the insufficient supply of lattice oxygen. The iron-based phases can be reduced to ferrous or even metallic iron states. Use of steam as a gasifying agent can also oxidize the low-valent iron phases to produce H_2 (typically the steam−iron reaction). This is advantageous for obtaining H_2-rich syngas products. Therefore, it is necessary to investigate the steam−iron reaction based on deeply reduced OCs (dre-OCs). The H_2 production rates of various dre-OCs are shown in Figure 10a. The results indicate that there is little difference between these samples in the initial increase of the H_2 production rate. After that, the rate curve of each sample declines slowly, during which period the H_2 production rates of dre-Fe100@C and dre-Cu20Fe80@C OCs are higher and last longer than those of the other two dre-OCs. This is due to higher Fe_2O_3 contents contained in Fe100@C and Cu20Fe80@C ($CuFe_2O_4$ is treated as CuO and Fe_2O_3) OCs. After all, the duration of H_2 production is directly related to the Fe-based phase content in the OC. This also explains why the time order of various dre-OCs in the H_2 production is dre-Cu10.9Red89.1@C < dre-red mud < dre-Cu20Fe80@C < dre-Fe100@C. The H_2 yield and reaction time (the number in parentheses) of each dre-OC are also calculated and presented in Figure 10b. It is observed that the H_2 yields of dre-Fe100@C and dre-Cu20Fe80@C OCs are 0.091 and 0.079 mol, respectively. These clearly exceed 0.038 mol with dre-red mud and 0.035 mol with dre-Cu10.9Red89.1@C. Additionally, the average H_2 production rate can be calculated by dividing the H_2 yield by the reaction time, and the values obtained are 4.4×10^{-5}, 4.6×10^{-5}, 2.9×10^{-5}, and 3.9×10^{-5} mol/s for dre-Fe100@C, dre-Cu20Fe80@C, dre-red mud, and dre-Cu10.9Red89.1@C, respectively.

To compare these samples under the same standard, the H_2 yield based on per mass of Fe_2O_3 (i.e., H_2 yield/the mass of Fe_2O_3) is also calculated for each OC. The results shown in Figure 10b indicate that the H_2 yields of dre-Fe100@C and dre-Cu20Fe80@C are similar as per mass Fe_2O_3 counted but significantly higher than those of the other two dre-OCs. The obviously higher H_2 yield of dre-Cu10.9Red89.1@C relative to dre-red mud based on per mass Fe_2O_3 may be derived from the contribution of Cu to the reduction of Fe-based phases during the reduction period.[46]

3.4. Cyclic Stability Tests. *3.4.1. Redox Cycles.* To examine the cyclic stability of the promising red mud and Cu20Fe80@C OCs, 8 redox cycles are performed in the batch fluidized bed reactor under the conditions of 950 °C, an O/C ratio of 0.2, and a steam concentration of 50 vol %. Figure 11a shows the gas compositions of these two OCs with increasing cycles. It is seen that both OCs obtain a stable gas distribution within 8 cycles, and the average reaction times during the cycle are 725 and 796 s for red mud and Cu20Fe80@C OCs, respectively. The syngas yields and H_2/CO ratios of these two OCs with cycles are presented in Figure 11b. As seen, in comparison to the syngas yield of red mud within the range of 1.08−1.14 Nm^3/kg of coal, the Cu20Fe80@C OC attains a higher syngas yield ranging from 1.25 to 1.29 Nm^3/kg of coal. Moreover, the H_2/CO ratios of Cu20Fe80@C are always higher than those of red mud during the cyclic tests. As such, the Cu20Fe80@C OC is a better candidate for the H_2-rich syngas production.

3.4.2. OC Characterization. Figure 12 compares the morphological and structural features of the fresh and used OCs of red mud and Cu20Fe80@C using ESEM. Two magnification levels of 300× and 1000× are selected for these two OCs. It is seen that Cu20Fe80@C presents an obviously rougher surface morphology and richer porous structure in comparison to red mud. For either OC, there is no obvious sintering phenomenon observed on the particle surface by

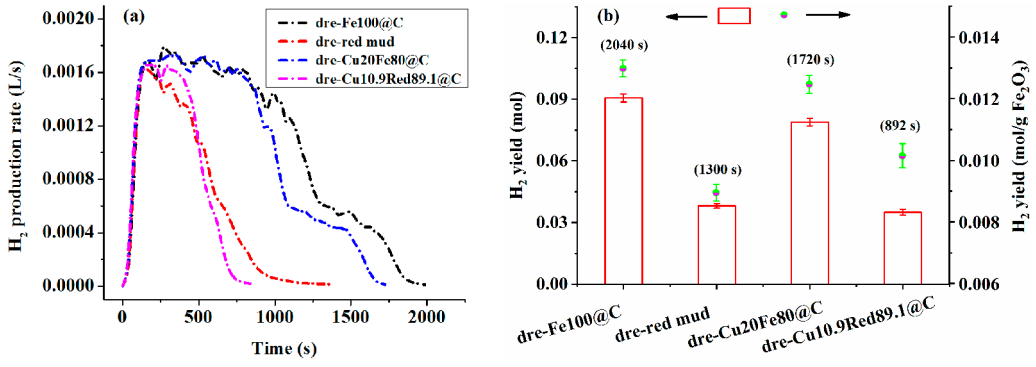

Figure 10. (a) H_2 production rate and (b) H_2 yield of different OCs (temperature, 950 °C; steam concentration, 40 vol %; the number in parentheses is the average reaction time for three repeated tests).

https://doi.org/10.1021/acs.energyfuels.1c01800
Energy Fuels 2021, 35, 15513−15524

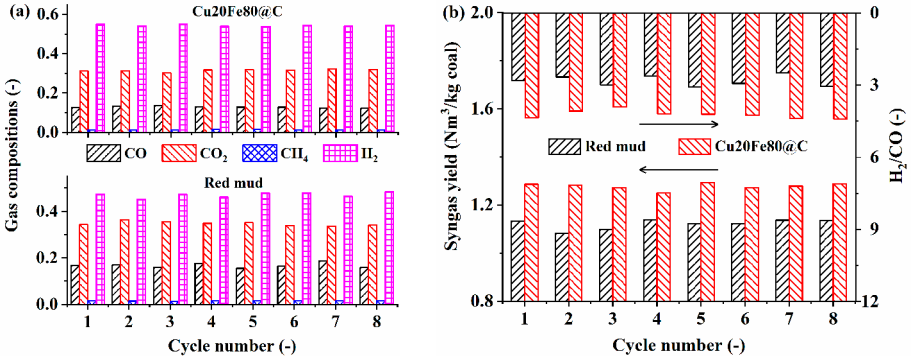

Figure 11. (a) Gas compositions and (b) syngas quality of red mud and Cu20Fe80@C OCs during the cyclic CLG tests (temperature, 950 °C; O/C ratio, 0.2; and steam concentration, 50 vol %).

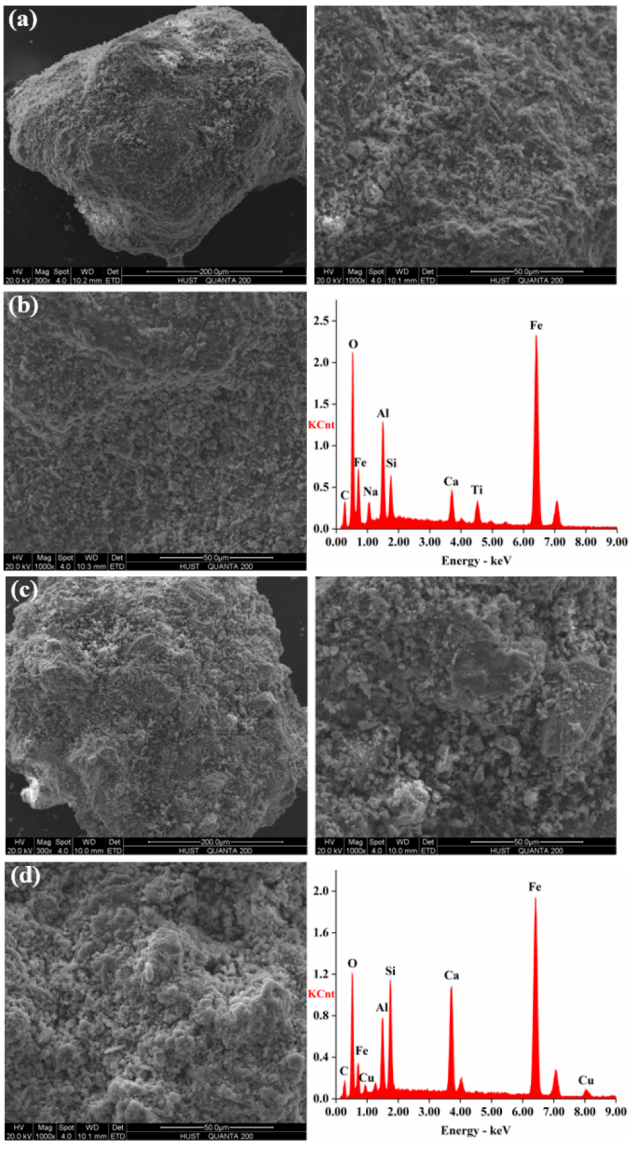

Figure 12. ESEM pictures of fresh (a) red mud and (c) Cu20Fe80@C particles and EDX analyses of used (b) red mud and (d) Cu20Fe80@C particles after cycles in CLG tests.

comparing the surface morphology of fresh and used particles (1000×). Moreover, the surface element distributions of the used particles are detected by employing EDX. The EDX results indicate that both OCs contain Fe, Al, Ca, Si, C, and O elements; however, additional Na and Ti are detected in red mud and additional Cu is detected in Cu20Fe80@C. It should be noted that the C element is derived from the pretreatment of carbon coating, which aims to enhance the electrical conductivity of the particle surface.

Table 6 lists the specific surface area, pre volume, and pore diameter of fresh and used OCs (after 8 redox cycles) measured by Brunauer–Emmett–Teller (BET). Decreasing values can be observed for used particles. This demonstrates that the porosity in used particles is decreased, which may be caused by ash deposition because no obvious sintering behavior is found in the particles (as presented in Figure 12). Moreover, the crushing strength (an average value of 30 measurements) is obtained using a digital dynamometer (FGP-100, Shimpo), with the values of 1.92 (±0.22) and 1.78 (±0.10) N for fresh and used Cu20Fe80@C OC, respectively, and 1.88 (±0.16) and 1.95 (±0.12) for fresh and used red mud OC, respectively.

4. CONCLUSION

In this work, the performance of low-cost OCs, prepared from waste ore particles and/or bauxite residues, are evaluated in the CLG mode. Both coal and char are used as fuels for the CLG investigation in a batch fluidized bed reactor. Moreover, the catalytic effects of reduced OCs on the WGS reaction and H_2 production charateristics of deeply reduced OC are investigated in a fixed bed reactor. The specific conclusions are as follows: (1) The coal CLG tests indicate that the copper-ore-containing OCs (i.e. Cu20Fe80@C and Cu10.9Red89.1@C) exhibit better reactivity with the volatiles/gasification gases in the combustion period of the CLG process. The Cu10.9Red89.1@C OC obtains a significantly lower syngas yield compared to red mud. However, it is not the case for Cu20Fe80@C, which attains a similar syngas yield with Fe100@C. With the coal gasification time and syngas quality taken into consideration, the red mud and Cu20Fe80@C OCs are better candidates and the H_2/CO ratios of 4.03 and 2.36 are attained, respectively, which are good for the H_2-rich chemical synthesis and the Fischer–Tropsch synthesis, respectively. A further increase in the weight ratio of copper ore/hematite in the OC from 20:80 is disadvantageous for syngas production. (2) The coal/char CLG tests indicate that both active lattice oxygen and alkali metal facilitate the coal/char conversion acceleration, which can be identified clearly from the instantaneous carbon conversion rate curves. By char tests of pulsed feeding, it is found that the char conversion rate is highly related to the H_2 yield, which is considered as the

https://doi.org/10.1021/acs.energyfuels.1c01800
Energy Fuels 2021, 35, 15513–15524

Table 6. Physical Property of the Fresh and Used OCs

	specific surface area (m^2/g)		total pore volume (cm^3/g)		average pore diameter (Å)	
OC	fresh	used	fresh	used	fresh	used
red mud	1.0566	0.9053	0.001959	0.001540	74.1603	65.3804
Cu20Fe80@C	1.5939	1.4842	0.003066	0.002648	76.9297	72.9244

inhibitor, while the reduced OCs can exert a catalytic function in producing H_2-rich syngas, which affects the char gasification rate as well as syngas quality. (3) With respect to the WGS reaction, the catalytic order of reduced OCs is determined as re-Cu20Fe80@C > re-Fe100@C > re-red mud. While for the steam−iron reaction, it is found that the H_2 production rates of dre-Fe100@C and dre-Cu20Fe80@C samples are higher and with a longer duration compared to the other two dre-OCs. Moreover, the H_2 yields of dre-Fe100@C and dre-Cu20Fe80@C are similar but significantly higher than those of the other two dre-OCs. (4) The cyclic redox tests show that both Cu20Fe80@C and red mud OCs can maintain a stable syngas yield within the range of 1.25−1.29 and 1.08−1.14 Nm^3/kg of coal, respectively. Moreover, the ESEM−EDX results indicate good anti-sintering behavior of both OCs. It is noted that the main purposes are to (1) screen out promising OCs for syngas production via CLG and (2) examine the role of OC on char gasification and syngas quality. The results obtained in the batched fluidized/fixed bed reactor are valuable for comparison purposes among different OCs as well as identifying the OC role. However, it is inferred that the CLG performance (including char gasification rate, syngas yield, syngas compositions, etc.) of OCs may be quite different in a continuous unit, which deserves comprehensive investigations in the future.

AUTHOR INFORMATION

Corresponding Author

Haibo Zhao − *State Key Laboratory of Coal Combustion, School of Energy and Power Engineering, Huazhong University of Science and Technology, Wuhan, Hubei 430074, People's Republic of China;* orcid.org/0000-0002-2693-4499; Phone: +86-27-8754-2417, ext. 8208; Email: hzhao@mail.hust.edu.cn; Fax: +86-27-8754-5526

Authors

Yanan Wang − *State Key Laboratory of Coal Combustion, School of Energy and Power Engineering, Huazhong University of Science and Technology, Wuhan, Hubei 430074, People's Republic of China*

Hengfeng Bu − *State Key Laboratory of Coal Combustion, School of Energy and Power Engineering, Huazhong University of Science and Technology, Wuhan, Hubei 430074, People's Republic of China*

Kunlei Liu − *Center for Applied Energy Research, University of Kentucky, Lexington, Kentucky 40511, United States;* orcid.org/0000-0003-3229-0260

Complete contact information is available at: https://pubs.acs.org/10.1021/acs.energyfuels.1c01800

Notes

The authors declare no competing financial interest.

ACKNOWLEDGMENTS

This work was supported by the National Key R&D Program of China (2019YFE0100100) and the National Natural Science Foundation of China (52025063). The authors are grateful to the Analytical and Testing Center of Huazhong University of Science and Technology (HUST) for XRD and ESEM−EDX measurements.

REFERENCES

(1) Stiegel, G. J.; Maxwell, R. C. Gasification technologies: The path to clean, affordable energy in the 21st century. *Fuel Process. Technol.* **2001**, *71*, 79−97.

(2) Fan, L.; Li, F.; Ramkumar, S. Utilization of chemical looping strategy in coal gasification processes. *Particuology* **2008**, *6*, 131−142.

(3) Wu, J.; Bai, L.; Tian, H.; Riley, J.; Siriwardane, R.; Wang, Z.; He, T.; Li, J.; Zhang, J.; Wu, J. Chemical looping gasification of lignin with bimetallic oxygen carriers. *Int. J. Greenhouse Gas Control* **2020**, *93*, 102897.

(4) Mattisson, T.; Keller, M.; Linderholm, C.; Moldenhauer, P.; Rydén, M.; Leion, H.; Lyngfelt, A. Chemical-looping technologies using circulating fluidized bed systems: Status of development. *Fuel Process. Technol.* **2018**, *172*, 1−12.

(5) Huang, X.; Wu, J.; Wang, M.; Ma, X.; Jiang, E.; Hu, Z. Syngas production by chemical looping gasification of rice husk using Fe-based oxygen carrier. *J. Energy Inst.* **2020**, *93*, 1261−1270.

(6) Samprón, I.; de Diego, L. F.; García-Labiano, F.; Izquierdo, M. T.; Abad, A.; Adánez, J. Biomass Chemical Looping Gasification of pine wood using a synthetic Fe_2O_3/Al_2O_3 oxygen carrier in a continuous unit. *Bioresour. Technol.* **2020**, *316*, 123908.

(7) Shen, T.; Wu, J.; Shen, L.; Yan, J.; Jiang, S. Chemical Looping Gasification of Coal in a 5 kW_{th} Interconnected Fluidized Bed with a Two-Stage Fuel Reactor. *Energy Fuels* **2018**, *32*, 4291−4299.

(8) Virginie, M.; Adánez, J.; Courson, C.; de Diego, L. F.; García-Labiano, F.; Niznansky, D.; Kiennemann, A.; Gayán, P.; Abad, A. Effect of Fe-olivine on the tar content during biomass gasification in a dual fluidized bed. *Appl. Catal., B* **2012**, *121*−*122*, 214−222.

(9) Condori, O.; García-Labiano, F.; de Diego, L. F.; Izquierdo, M. T.; Abad, A.; Adánez, J. Biomass chemical looping gasification for syngas production using ilmenite as oxygen carrier in a 1.5 kW_{th} unit. *Chem. Eng. J.* **2021**, *405*, 126679.

(10) Tsedenbal, B.; Kannari, N.; Sato, K.; Abe, H.; Shirai, H.; Takarada, T. Reforming of coal volatiles over ilmenite ore. *Fuel Process. Technol.* **2019**, *192*, 96−104.

(11) Lind, F.; Berguerand, N.; Seemann, M.; Thunman, H. Ilmenite and Nickel as Catalysts for Upgrading of Raw Gas Derived from Biomass Gasification. *Energy Fuels* **2013**, *27*, 997−1007.

(12) Larsson, A.; Israelsson, M.; Lind, F.; Seemann, M.; Thunman, H. Using Ilmenite To Reduce the Tar Yield in a Dual Fluidized Bed Gasification System. *Energy Fuels* **2014**, *28*, 2632−2644.

(13) Keller, M.; Leion, H.; Mattisson, T.; Thunman, H. Investigation of Natural and Synthetic Bed Materials for Their Utilization in Chemical Looping Reforming for Tar Elimination in Biomass-Derived Gasification Gas. *Energy Fuels* **2014**, *28*, 3833−3840.

(14) Wang, Z.; Zhu, M.; He, T.; Zhang, J.; Wu, J.; Tian, H.; Wu, J. Chemical looping reforming of toluene as a biomass tar model compound over two types of oxygen carriers: $2CuO−2NiO/Al_2O_3$ and $CaFe_2O_4$. *Fuel* **2018**, *222*, 375−384.

(15) Siriwardane, R.; Riley, J.; Tian, H.; Richards, G. Chemical looping coal gasification with calcium ferrite and barium ferrite via solid-solid reactions. *Appl. Energy* **2016**, *165*, 952−966.

(16) Chen, J.; Zhao, K.; Zhao, Z.; He, F.; Huang, Z.; Wei, G. Identifying the roles of MFe_2O_4 (M = Cu, Ba, Ni, and Co) in the chemical looping reforming of char, pyrolysis gas and tar resulting from biomass pyrolysis. *Int. J. Hydrogen Energy* **2019**, *44*, 4674−4687.

(17) He, F.; Huang, Z.; Wei, G.; Zhao, K.; Wang, G.; Kong, X.; Feng, Y.; Tan, H.; Hou, S.; Lv, Y.; Jiang, G.; Guo, Y. Biomass chemical-looping gasification coupled with water/CO_2-splitting using $NiFe_2O_4$ as an oxygen carrier. *Energy Convers. Manage.* **2019**, *201*, 112157.
(18) Huang, Z.; Deng, Z.; Feng, Y.; Chen, T.; Chen, D.; Zheng, A.; Wei, G.; He, F.; Zhao, Z.; Wu, J.; Li, H. Exploring the Conversion Mechanisms of Toluene as a Biomass Tar Model Compound on $NiFe_2O_4$ Oxygen Carrier. *ACS Sustainable Chem. Eng.* **2019**, *7*, 16539−16548.
(19) Kun, Z.; He, D.; Guan, J.; Wang, Q.; Li, X.; Shang, J.; Zhang, Q. Interaction between bimetallic composite oxygen carriers and coal and its contribution to coal direct chemical looping gasification. *Int. J. Hydrogen Energy* **2020**, *45*, 19052−19066.
(20) Shen, T.; Ge, H.; Shen, L. Characterization of combined Fe-Cu oxides as oxygen carrier in chemical looping gasification of biomass. *Int. J. Greenhouse Gas Control* **2018**, *75*, 63−73.
(21) Tian, X.; Niu, P.; Ma, Y.; Zhao, H. Chemical-looping gasification of biomass: Part II. Tar yields and distributions. *Biomass Bioenergy* **2018**, *108*, 178−189.
(22) Kun, Z.; He, D.; Guan, J.; Shan, L.; Wu, Z.; Zhang, Q. Coal gasification using chemical looping with varied metal oxides as oxygen carriers. *Int. J. Hydrogen Energy* **2020**, *45*, 10696−10708.
(23) Su, M.; Tian, X.; Zhao, H. Particle-resolved simulation and modeling of the conversion rate of coal char in chemical looping with oxygen uncoupling. *Combust. Flame* **2020**, *213*, 331−342.
(24) Su, M.; Zhao, H. A modified intrinsic model for conversion rate of coal char particle in chemical looping with oxygen uncoupling conditions. *Fuel* **2021**, *288*, 119615.
(25) Siriwardane, R.; Tian, H.; Richards, G.; Simonyi, T.; Poston, J. Chemical-Looping Combustion of Coal with Metal Oxide Oxygen Carriers. *Energy Fuels* **2009**, *23*, 3885−3892.
(26) Pérez-Vega, R.; Abad, A.; Gayán, P.; de Diego, L. F.; García-Labiano, F.; Adánez, J. Development of $(Mn_{0.77}Fe_{0.23})_2O_3$ particles as an oxygen carrier for coal combustion with CO_2 capture via in-situ gasification chemical looping combustion (*i*G-CLC) aided by oxygen uncoupling (CLOU). *Fuel Process. Technol.* **2017**, *164*, 69−79.
(27) Su, M.; Zhao, H.; Tian, X. The competition between direct gas-solid reduction and oxygen uncoupling of CuO oxygen carrier in chemical looping with oxygen uncoupling: A single particle simulation study. *Combust. Flame* **2020**, *221*, 219−227.
(28) Zhao, H.; Tian, X.; Ma, J.; Chen, X.; Su, M.; Zheng, C.; Wang, Y. Chemical Looping Combustion of Coal in China: Comprehensive Progress, Remaining Challenges, and Potential Opportunities. *Energy Fuels* **2020**, *34*, 6696−6734.
(29) Cho, P.; Mattisson, T.; Lyngfelt, A. Comparison of iron-, nickel-, copper- and manganese-based oxygen carriers for chemical-looping combustion. *Fuel* **2004**, *83*, 1215−1225.
(30) Xu, T.; Xu, F.; Moyo, G. G.; Sun, Y.; Chen, Z.; Xiao, B.; Wang, X.; Hu, Z. Comparative study of M_xO_y (M = Cu, Fe and Ni) supported on dolomite for syngas production via chemical looping reforming with toluene. *Energy Convers. Manage.* **2019**, *199*, 111937.
(31) Niu, P.; Ma, Y.; Tian, X.; Ma, J.; Zhao, H. Chemical looping gasification of biomass: Part I. screening Cu-Fe metal oxides as oxygen carrier and optimizing experimental conditions. *Biomass Bioenergy* **2018**, *108*, 146−156.
(32) Yang, J.; Cai, N.; Li, Z. Reduction of Iron Oxide as an Oxygen Carrier by Coal Pyrolysis and Steam Char Gasification Intermediate Products. *Energy Fuels* **2007**, *21*, 3360−3368.
(33) Wang, L.; Shen, L.; Jiang, S.; Song, T. Chemical looping gasification with potassium-catalyzed petroleum coke for enhanced production of H_2 and H_2S. *Chem. Eng. J.* **2020**, *397*, 124631.
(34) Guo, Q.; Cheng, Y.; Liu, Y.; Jia, W.; Ryu, H. Coal Chemical Looping Gasification for Syngas Generation Using an Iron-Based Oxygen Carrier. *Ind. Eng. Chem. Res.* **2014**, *53*, 78−86.
(35) Chen, L.; Yang, L.; Liu, F.; Nikolic, H. S.; Fan, Z.; Liu, K. Evaluation of multi-functional iron-based carrier from bauxite residual for H_2-rich syngas production via chemical-looping gasification. *Fuel Process. Technol.* **2017**, *156*, 185−194.
(36) Arjmand, M.; Leion, H.; Mattisson, T.; Lyngfelt, A. Investigation of different manganese ores as oxygen carriers in chemical-looping combustion (CLC) for solid fuels. *Appl. Energy* **2014**, *113*, 1883−1894.
(37) Wang, Y.; Tian, X.; Zhao, H.; Liu, K. The use of a low-cost oxygen carrier prepared from red mud and copper ore for in situ gasification chemical looping combustion of coal. *Fuel Process. Technol.* **2020**, *205*, 106460.
(38) Tian, X.; Zhao, H.; Ma, J. Cement bonded fine hematite and copper ore particles as oxygen carrier in chemical looping combustion. *Appl. Energy* **2017**, *204*, 242−253.
(39) Zhao, H.; Tian, X.; Ma, J.; Su, M.; Wang, B.; Mei, D. Development of tailor-made oxygen carriers and reactors for chemical looping processes at Huazhong University of Science & Technology. *Int. J. Greenhouse Gas Control* **2020**, *93*, 102898.
(40) Wang, Y.; Tian, X.; Zhao, H.; Liu, K.; Dong, Y.; Su, Z.; Zheng, C. Synergetic effects of cement bonded copper ore and red mud as oxygen carrier during *in-situ* gasification chemical looping combustion of coal char. *Fuel* **2021**, *303*, 121295.
(41) Wang, Y.; Niu, P.; Zhao, H. Chemical looping gasification of coal using calcium ferrites as oxygen carrier. *Fuel Process. Technol.* **2019**, *192*, 75−86.
(42) Su, Z.; Wang, Y.; Du, H.; Ma, J.; Zheng, Y.; Zhao, H. Using Copper Ore and Hematite Fine Particles as Raw Materials of an Oxygen Carrier for Chemical Looping Combustion of Coal: Spray Drying Granulation and Performance Evaluation. *Energy Fuels* **2020**, *34*, 8587−8599.
(43) Huang, Z.; Deng, Z.; Chen, D.; Wei, G.; He, F.; Zhao, K.; Zheng, A.; Zhao, Z.; Li, H. Exploration of Reaction Mechanisms on Hydrogen Production through Chemical Looping Steam Reforming Using $NiFe_2O_4$ Oxygen Carrier. *ACS Sustainable Chem. Eng.* **2019**, *7*, 11621−11632.
(44) Keller, M.; Leion, H.; Mattisson, T.; Lyngfelt, A. Gasification inhibition in chemical-looping combustion with solid fuels. *Combust. Flame* **2011**, *158*, 393−400.
(45) Hildor, F.; Leion, H.; Linderholm, C. J.; Mattisson, T. Steel converter slag as an oxygen carrier for chemical-looping gasification. *Fuel Process. Technol.* **2020**, *210*, 106576.
(46) Wang, B.; Ma, Q.; Wang, W.; Zhang, C.; Mei, D.; Zhao, H.; Zheng, C. Effect of Reaction Temperature on the Chemical Looping Combustion of Coal with $CuFe_2O_4$ Combined Oxygen Carrier. *Energy Fuels* **2017**, *31*, 5233−5245.

https://doi.org/10.1021/acs.energyfuels.1c01800
Energy Fuels 2021, 35, 15513−15524